

Activation of silicon implanted with phosphorus and boron atoms by microwave annealing with carbon powder as a heat source

Masahiko Hasumi, Tomohiko Nakamura, Shinya Yoshidomi, and Toshiyuki Sameshima*

Tokyo University of Agriculture and Technology, Koganei, Tokyo 184-8588, Japan
E-mail: tsamesim@cc.tuat.ac.jp

Received November 1, 2013; accepted February 28, 2014; published online April 18, 2014

We report the activation of silicon implanted with phosphorus and boron atoms by microwave annealing using carbon powder as a heat source. Silicon substrates were covered with carbon powder and then irradiated with 2.45 GHz microwaves using a commercial microwave oven. Carbon powder effectively absorbs microwaves and heats itself at 1000 °C. Silicon substrates are heated by thermal conduction. We carried out implantations of phosphorus atoms at a concentration of $1.0 \times 10^{15} \text{ cm}^{-2}$ at 75 keV and boron atoms at a concentration of $1.0 \times 10^{15} \text{ cm}^{-2}$ at 25 keV for p- and n-type silicon substrates, respectively. Microwave annealing at 1000 W for 120 s achieved sheet resistivities of 140 and 85 Ω/sq for the phosphorus- and boron-implanted samples, respectively. It also realized the recrystallization of surface amorphized regions caused by implantation. Moreover, low surface recombination velocities of 3.8×10^2 and $2.7 \times 10^2 \text{ cm/s}$ were obtained at the top implanted surfaces for the phosphorus- and boron-implanted samples, respectively. Typical diode rectified characteristics and solar cell characteristics with a conversion efficiency of 10.1% were successfully obtained. © 2014 The Japan Society of Applied Physics

1. Introduction

The activation of semiconductor materials implanted with impurity atoms is important for the fabrication of devices, such as metal oxide semiconductor field effect transistors (MOSFETs), pn junction diodes, and solar cells.¹⁻⁴⁾ In particular, rapid heating is an attractive method for activating a semiconductor because it is important to reduce the thermal budget for fabricating semiconductor devices at a low cost. A high activation ratio and no marked impurity diffusion are also important for fabricating an extremely shallow junction. Many studies have proved the advantages of rapid heating.⁵⁻¹⁰⁾ We have also investigated continuous wave infrared semiconductor laser annealing using a carbon layer as an optical absorption layer.^{11,12)} The infrared semiconductor laser is attractive for heating processes with high throughput because of its high power, high conversion efficiency, and stable emission. To solve the problem of the low optical absorbance of silicon in the infrared region, we used carbon as a photo-absorption layer. A black carbon layer with a high heat resistivity can serve as a heat source at high temperatures.¹³⁾ It has an important role in effectively heating silicon substrates and achieving a complete activation of implanted impurities. Microwave heating is also attractive for the rapid heating method.^{14,15)} Recently, we have reported a simple thermal annealing method using a commercial 2.45 GHz microwave oven.¹⁶⁾ Thermal annealing is important for reducing the number of defects generated during device fabrication processes. We demonstrated the curing of severe carrier recombination defects caused by argon plasma irradiation.^{16,17)} Microwave annealing was conducted with 2-mm-thick glass substrates, which sandwiched a silicon sample to maintain the thermal energy in silicon and realize gradual cooling. However, there is a difficulty in achieving a sufficiently high temperature for activating the implanted impurity atoms with low thermal budget, because the microwave reflection is enhanced by the increase in the conductivity of silicon substrates with thermally generated intrinsic carriers at high temperatures.

In this paper, we report the activation of silicon implanted with phosphorus and boron atoms by microwave annealing with carbon powder as a heat source. Silicon substrates were

completely covered with carbon powder for effective heating and irradiated with microwaves using a commercial 2.45 GHz microwave oven. Carbon powder effectively absorbs microwaves and heats itself at 1000 °C. Silicon substrates are heated by thermal conduction. This is a similar concept of our previous research on infrared semiconductor laser annealing with a carbon photo-absorption layer. First, we examined the recrystallization properties of the disordered amorphous regions formed by the phosphorus and boron implantations. We then investigated the activation of phosphorus and boron atoms using a 9.35 GHz microwave transmittance measurement system. Moreover, to investigate the change in the density of surface recombination defect states at the top implanted region, we induced continuous wave (CW) 635 and 980 nm light illuminations to the system of microwave transmittance measurement. Finally, we demonstrated the diode rectified characteristics and solar cell characteristics for the sample activated by the present method.

2. Experimental procedure

15 $\Omega \text{ cm}$ p-type silicon substrates with a thickness of 500 μm were prepared. The top and rear surfaces were coated with 100-nm-thick thermally grown SiO_2 layers. The ion implantation of phosphorus atoms was conducted for the top surface of silicon substrates. The acceleration energy was set at 75 keV to have the peak concentration at the interface of thermally grown SiO_2 and silicon. The total dose was $2.0 \times 10^{15} \text{ cm}^{-2}$. Phosphorus atoms at a concentration of $1.0 \times 10^{15} \text{ cm}^{-2}$ were effectively implanted in silicon substrates. We also conducted the ion implantation of boron atoms at 25 keV to 7 $\Omega \text{ cm}$, 500- μm -thick n-type silicon substrates coated with 100-nm-thick thermally grown SiO_2 layers. Boron atoms at a concentration of $1.0 \times 10^{15} \text{ cm}^{-2}$ were effectively implanted in silicon substrates. The implanted samples were subsequently heat-treated by microwave irradiation using a commercial 2.45 GHz microwave oven at 1000 W for a duration ranging from 60 to 180 s. The silicon substrates were completely covered with carbon powder for effective heating and placed on a glass substrate with low heat conductivity to keep the heated energy in the sample region.¹⁸⁾ The glass substrate also protected the oven mechanics from the high temperature during heating.

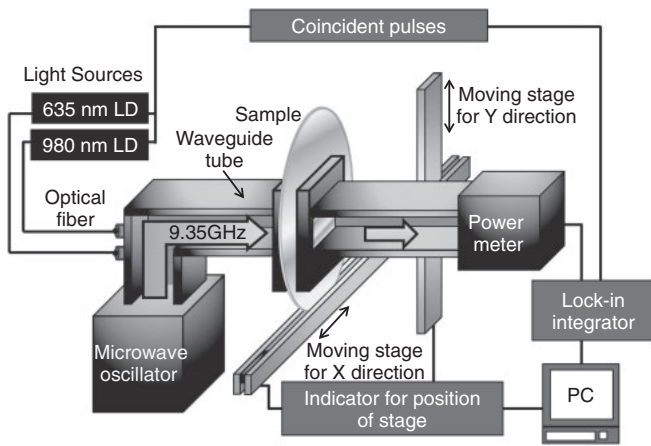


Fig. 1. Schematic apparatus for a 9.35 GHz microwave transmittance measurement system with 635 and 980 nm light illuminations.

Optical reflectivity spectra were measured using a conventional spectrometer to investigate the crystalline state in the implanted surface region in order to analyze the in-depth distribution of crystalline volume ratio by a numerical calculation program using the Fresnel optical interference effect.^{19,20} Photo-induced minority carrier annihilation behavior was also investigated using a 9.35 GHz microwave transmittance measurement system with waveguide tubes, which had a narrow gap for placing a sample, as shown by a schematic apparatus in Fig. 1.^{21–23} Continuous wave (CW) 635 and 980 nm laser diode (LD) lights were introduced to the waveguide tube. The light intensities on the sample surface were set at 1.5 and 0.98 mW/cm², respectively, for 635 and 980 nm lights to realize the same photon flux between the two different wavelength lights. The microwaves transmitted by the samples were rectified using a high-speed diode and integrated. The activation of impurity atoms was investigated on the basis of the sheet resistivity of the samples analyzed from the microwave transmittance in the dark field. The effective minority carrier lifetime (τ_{eff}) of the samples was analyzed from the detected microwave intensity under light illumination and in the dark field. We constructed a finite element numerical calculation program including theories of carrier generation associated with optical absorption coefficients, carrier diffusion, and annihilation for estimating the surface recombination velocity at the top surface S_{top} , and rear surface S_{rear} , and the bulk lifetime τ_b . The most possible S_{top} and S_{rear} were determined by the best coincidence between experimental and calculated τ_{eff} values.^{24–26}

To demonstrate the diode rectified characteristics and solar cell characteristics, the sample structured with a p-doped region/n-type silicon substrate/n+-doped region was fabricated by the present annealing method. 7 Ω cm n-type silicon substrates with a thickness of 500 μ m were prepared. The top and rear surfaces were coated with 100-nm-thick thermally grown SiO₂ layers. The ion implantation of boron atoms at a concentration of 1.0×10^{15} cm⁻² at 25 keV was conducted for the top silicon surface and that of phosphorus atoms at a concentration of 1.0×10^{15} cm⁻² at 75 keV was conducted for the rear silicon surface. The sample was covered with carbon powder and subsequently heat-treated by microwave irradiation at 1000 W for 120 s. The thermally

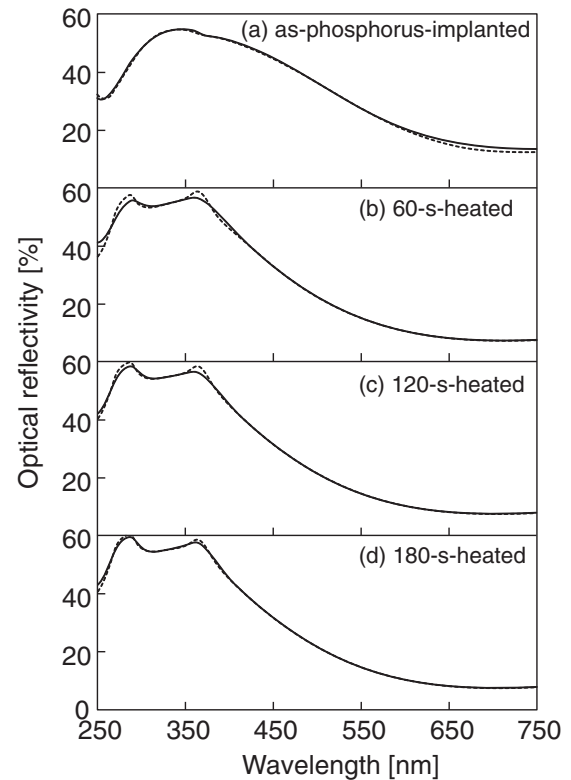


Fig. 2. Optical reflectivity spectra for samples (a) as-implanted with phosphorus at a concentration of 1.0×10^{15} cm⁻², and microwave-annealed for (b) 60, (c) 120, and (d) 180 s. The calculated spectra are also presented (dashed curves).

grown SiO₂ layer was removed using hydrofluoric acid. Comb-type Al electrodes were formed on the top surface and the rear surface was entirely coated with Al electrodes by vacuum evaporation. The electrical current as a function of voltage (I - V) was measured using air mass (AM) 1.5 light at 100 W/cm².

3. Results and discussion

3.1 Recrystallization of doped region

Figure 2 shows optical reflectivity spectra for the phosphorus-implanted p-type silicon samples (a) as-implanted and microwave-annealed for (b) 60, (c) 120, and (d) 180 s. The samples were coated with 100-nm-thick thermally grown SiO₂ layers. Therefore, the optical interference effects of the SiO₂ layers were included in the obtained reflectivity spectra. The optical reflectivity for the as-implanted sample showed a broad spectrum, as shown in Fig. 2(a). There was no E₁ or E₂ peak in the ultraviolet region. These results indicate that the surface region was completely amorphized by phosphorus implantation. For the microwave-annealed samples, the E₁ and E₂ peaks appeared at approximately 370 and 280 nm, respectively. These peaks became larger as the duration of microwave irradiation increased. These results clearly indicate that the surface region was recrystallized by microwave annealing. Figure 2 also shows the numerically calculated spectra (dashed curves) constructed with the optical interference effect for a structure of multilayered silicon with different thickness and different crystalline volume ratios.¹⁹ Although we believe that the calculated spectra agreed well with experimental spectra, they were not

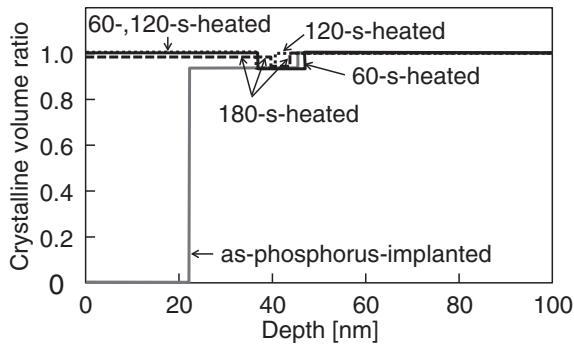


Fig. 3. In-depth distribution of crystalline volume ratio for samples as-implanted with phosphorus atoms and microwave-annealed for 60, 120, and 180 s obtained from the fitting process of the experimental and calculated optical reflectivity spectra given in Fig. 2.

perfectly coincident. The small differences between the calculated and experimental spectra shown in Fig. 2 probably occurred owing to the difference between the complex refractive indexes of amorphized silicon caused by implantation and those used for calculation. Our many fitting works suggest that the uncertainty of the complex refractive indexes of amorphized silicon caused by implantation results in the accuracy of our analysis of crystalline volume ratio within 10%.

Figure 3 shows changes in the in-depth distribution of the crystalline volume ratio for the phosphorus-implanted samples obtained from the best fitting between the experimental and calculated optical reflectivity spectra. For the phosphorus implantation at 75 keV, the 22-nm-deep region with respect to the silicon surface was completely amorphized. The partially amorphized region with a crystalline volume ratio of 0.94 was distributed from 22 to 45 nm depths from the silicon surface. The depth of the amorphized region was in rough agreement with the half width at half maximum (HWHM) for the in-depth distribution of implanted phosphorus atoms estimated by the Monte Carlo numerical calculation program of Stopping and Range of Ions in Matter (SRIM).²⁷⁾ The crystalline volume ratio of the 37-nm-deep surface region was restored to 1.00 for all the microwave-annealed samples. The surface regions of silicon were completely recrystallized, although partially amorphized regions with a crystalline volume ratio ranging from 0.94 to 0.95 were still distributed from 37 to 46 nm depths from the silicon surface.

Figure 4 shows the changes in the in-depth distribution of the crystalline volume ratio of n-type silicon samples implanted with boron atoms at a concentration of $1 \times 10^{15} \text{ cm}^{-2}$ at 25 keV obtained from the fitting process of the experimental and calculated optical reflectivity spectra. The 4-nm-deep region with respect to the silicon surface was amorphized at a crystalline volume ratio of 0.15 by boron implantation. Partially amorphized regions with a crystalline volume ratio ranging from 0.94 to 0.96 were distributed from 4 to 61 nm depths from the silicon surface. The crystalline volume ratio of the 4-nm-deep surface region was increased to 0.81 by microwave annealing for 90 and 120 s. On the other hand, the crystalline volume ratio of the surface region slightly decreased to 0.75 for the sample microwave-annealed

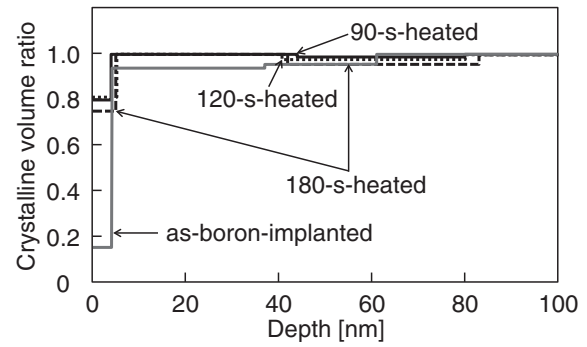


Fig. 4. In-depth distribution of crystalline volume ratio for samples as-implanted with boron atoms and microwave-annealed for 90, 120, and 180 s.

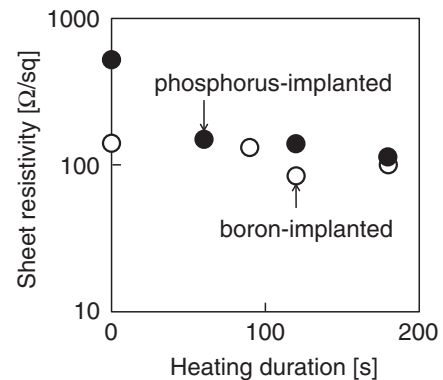


Fig. 5. Sheet resistivities of phosphorus- and boron-implanted samples as a function of microwave annealing duration.

for 180 s. Microwave annealing caused the recrystallization of boron-implanted surface regions as well as phosphorus-implanted samples.

3.2 Activation of dopant atoms

Figure 5 shows the sheet resistivities of phosphorus- and boron-implanted samples as a function of heating duration obtained by the analysis of the 9.35 GHz microwave transmittance measurement. The sheet resistivity of the phosphorus-as-implanted sample was $530 \text{ } \Omega/\text{sq}$. It was decreased to 150, 140, and $110 \text{ } \Omega/\text{sq}$ by microwave annealing for 60, 120, and 180 s, respectively, because of the increase in carrier density in the phosphorus-implanted region. The sheet resistivity of the boron-as-implanted sample was $140 \text{ } \Omega/\text{sq}$. It was also decreased to 130, 85, and $100 \text{ } \Omega/\text{sq}$ by microwave annealing for 90, 120, and 180 s, respectively. The carbon powder effectively absorbed the 2.45 GHz microwave and the silicon substrates were heated by heat conduction from the carbon powder during the operation of the microwave oven. Although the temperature increase of the silicon substrates was not precisely measured, the light emission from the carbon powder governed by the black body radiation rule indicated that the carbon powder was heated at $1000 \text{ } ^\circ\text{C}$ for the 1000 W microwave irradiation treatment for 120 s. Both phosphorus- and boron-implanted samples were effectively heated to high temperatures sufficient for moving the implanted atoms from interstitial sites to lattice sites. The activation ratio was estimated in the cases of minimum sheet resistivities. The minimum sheet

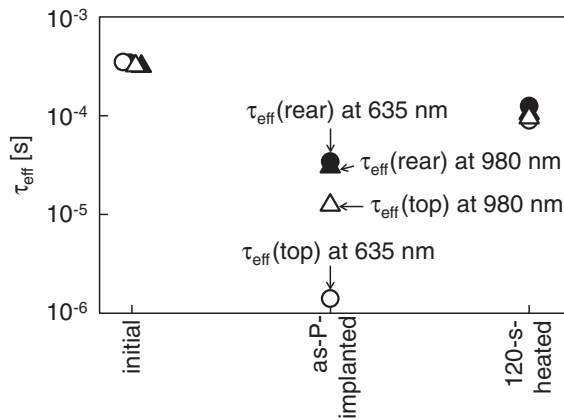


Fig. 6. Changes in τ_{eff} with phosphorus implantation followed by microwave annealing in the cases of four different light illumination modes. Circles and triangles show the 635 and 980 nm light illumination modes, respectively. Open and solid symbols show the top and rear surface illumination modes, respectively.

resistivities of the doped regions were obtained as 139 and 216 Ω/sq from the total minimum sheet resistivities of 110 and 85 Ω/sq for the phosphorus- and boron-implanted samples given above. The activation ratios were obtained as 0.64 and 0.87 from the ratios of the experimental minimum sheet resistivities to the theoretical sheet resistivities calculated with the carrier concentration distribution determined by SRIM²⁷⁾ and the carrier mobilities of doped crystalline silicon.²⁸⁾

3.3 Investigation of surface recombination defect states

The change in the τ_{eff} of the samples by microwave annealing was investigated. The τ_{eff} was investigated in the cases of 635 and 980 nm light illuminations to the top and rear surfaces. The τ_{eff} of the initial p-type silicon substrates coated with 100-nm-thick thermally grown SiO_2 layers, as-implanted with phosphorus atoms, and subsequently microwave-annealed at 1000 W for 120 s are shown in Fig. 6. Figure 7 also shows the τ_{eff} of the initial n-type silicon substrates coated with 100-nm-thick thermally grown SiO_2 layers, as-implanted with boron atoms, and subsequently microwave-annealed at 1000 W for 120 s. The initial p- and n-type silicon substrates coated with 100-nm-thick thermally grown SiO_2 layers had large τ_{eff} of 3.3×10^{-4} and 1.7×10^{-3} s in all light illumination cases, as shown in Figs. 6 and 7. No difference in τ_{eff} was observed in the cases of top and rear surface illuminations. These results indicate that both the top and rear silicon surfaces were well passivated by the thermally grown SiO_2 layers. The calculation result supports that small S_{top} and S_{rear} resulted in the same τ_{eff} in the cases of 635 and 980 nm light illuminations. The τ_{eff} of the phosphorus-as-implanted sample markedly decreased to 1.4×10^{-6} and 1.3×10^{-5} s in the cases of 635 and 980 nm light illuminations to the top surface, respectively, as shown in Fig. 6. This result shows that a substantial number of recombination defect states were generated in the silicon surface region by phosphorus implantation. The τ_{eff} in the case of 980 nm light illumination to the top surface was larger than that in the case of 635 nm light illumination, because the diffusion time was necessary for carriers generated in the

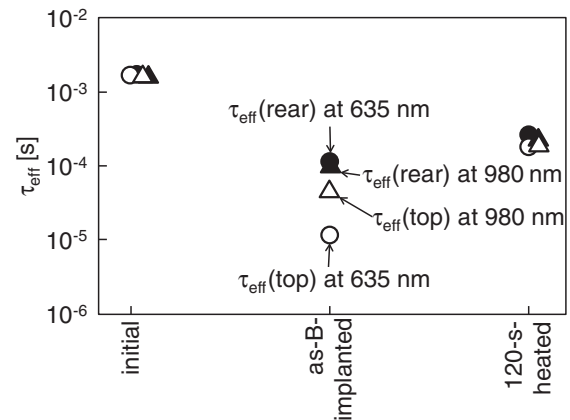


Fig. 7. Changes in τ_{eff} with boron implantation followed by microwave annealing in the cases of four different light illumination modes.

deep region by 980 nm light illumination to reach the top defective surface. The penetration depth at 635 nm was about 3 μm , while it was very large (125 μm) for 980 nm light.²⁹⁾ The photo-induced carriers generated in the deep region of semiconductors are active until they meet carrier recombination defect states when a high density of carrier recombination defect states is localized at the surface regions. Therefore, the τ_{eff} is large when carrier generation occurs in a deep region far from the surface. On the other hand, the τ_{eff} is small when carrier generation occurs close to the carrier recombination defect states. The τ_{eff} of the phosphorus-as-implanted sample in the cases of 635 and 980 nm light illuminations to the rear surface were 3.6×10^{-5} and 3.0×10^{-5} s, respectively. They were larger than those in the cases of light illuminations to the top surface, because the rear surface was well passivated by the thermally grown SiO_2 layer. The τ_{eff} in the case of 635 nm light illumination to the rear surface was larger than that in the case of 980 nm light illumination to the rear surface. This was also due to the difference in diffusion time to reach the top surface. The τ_{eff} of the sample subsequently treated by 2.45 GHz microwave irradiation at 1000 W for 120 s markedly increased. The τ_{eff} of the sample treated by 120 s microwave irradiation were 9.9×10^{-5} and 1.2×10^{-4} s, respectively, in the cases of 635 nm light illumination to the top and rear surfaces. The τ_{eff} in the case of 980 nm light illumination was almost the same as that in the case of 635 nm light illumination. The change in the τ_{eff} of the boron-implanted samples was essentially the same as that of the phosphorus-implanted samples, as shown in Fig. 7.

We analyzed the surface recombination velocity at the top implanted surface S_{top} and rear surface S_{rear} , and the bulk lifetime τ_b by using a finite element numerical calculation program. The most possible S_{top} and S_{rear} were determined by the best coincidence between the experimental and calculated τ_{eff} values. Figure 8 shows the carrier recombination velocity at the implanted surface S_{top} for the initial, as-implanted, and 120 s microwave-annealed samples. The S_{top} and S_{rear} of the initial p- and n-type silicon samples were 7.0 and 3.0 cm/s, respectively. The low surface recombination velocity was caused by the thermally grown SiO_2 layers formed on the top and rear surfaces. On the other hand, the S_{top} of the phosphorus-as-implanted sample was increased to 5.0×10^4

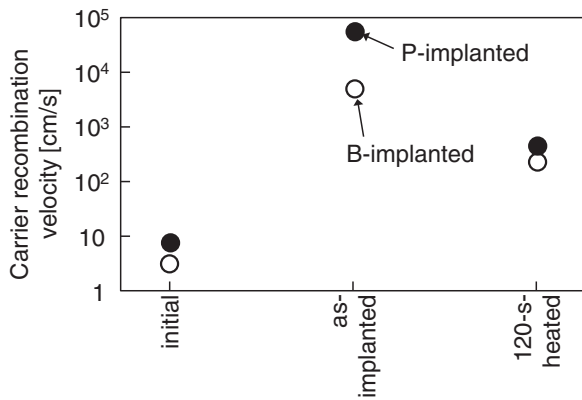


Fig. 8. Changes in carrier recombination velocities at the phosphorus- and boron-implanted surfaces.

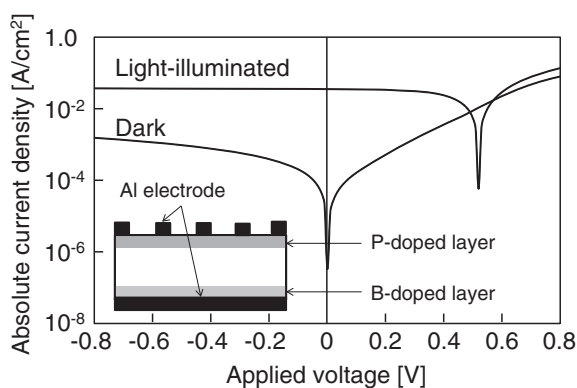


Fig. 9. Logarithmic plot of absolute electrical current density as a function of voltage for the microwave-annealed n-type silicon sample implanted with boron at the top surface and phosphorus at the rear surface. The sample structure is shown in the inset.

cm/s by the generation of defect states in the implanted region, while S_{rear} was kept at 7.0 cm/s. The S_{top} of the boron-as-implanted sample was also increased to 5.0×10^3 cm/s, while S_{rear} was kept at 3.0 cm/s. S_{top} was decreased to 3.8×10^2 and 2.7×10^2 cm/s for the phosphorus- and boron-implanted samples subsequently treated by microwave irradiation for 120 s, respectively. All the substrates cooled down after the termination of the microwave irradiation. The glass substrate served as a thermal insulator because of its low heat conductivity. We believe that gradual cooling was achieved at a low rate, which is essential for realizing a low density of defect states.³⁰⁾

3.4 Electrical characteristics

Figure 9 shows logarithmic plots of absolute electrical current density as a function of voltage when the sample was in the dark and illuminated with AM 1.5 light. The sample structure was boron-doped layer/n-type substrate/phosphorus-doped layer, as shown in the inset, and was activated by microwave annealing at 1000 W for 120 s with carbon powder. Typical diode rectified characteristics were observed in the dark, as shown in Fig. 9. Light illumination generated photo-induced current. The photo-induced current at 0 V, which corresponded to short circuit current density, was 36 mA/cm². Figure 10 shows solar cell characteristics of

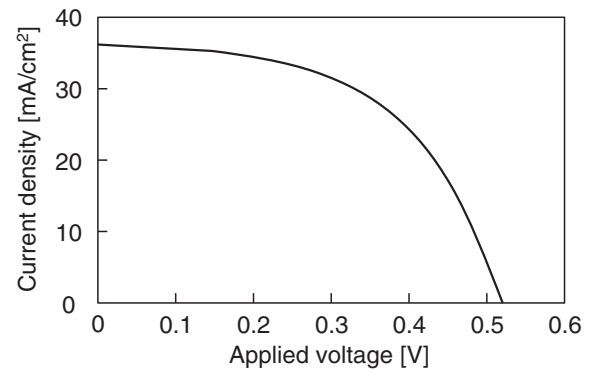


Fig. 10. Solar cell characteristics of the sample obtained from the I - V characteristics shown in Fig. 9.

the sample obtained from the I - V characteristics shown in Fig. 9. Typical solar cell current voltage characteristics were obtained. The short circuit current density I_{sc} , open circuit voltage V_{oc} , fill factor FF, and conversion efficiency were 36 mA/cm², 0.52 V, 0.54, and 10.1%, respectively. These results indicate that boron-doped regions were activated well and the built-in potential was formed well in the depletion regions under the top doped layers. The solar cell characteristics were acceptable when taking into account the low dose of 1×10^{15} cm⁻², the absence of the texture structure, surface passivation and antireflection, and the thick substrate thickness of 500 μm .

The experimental results shown in Figs. 2–10 demonstrated the activation of silicon implanted with phosphorus and boron atoms by microwave annealing with carbon powder as a heat source. Carbon powder effectively absorbed microwaves and silicon samples covered with carbon powder were effectively heated to activate the implanted impurity atoms by thermal conduction. Gradual cooling was also achieved by the underlying glass substrate because of its low heat conductivity. Therefore, a relatively low density of defect states at the top implanted region was achieved simultaneously. The commercial microwave oven currently limits the sample size to 4 in. for an effective heat treatment probably because of the temperature distribution. That problem will be overcome by further technical investigation. The present method will be useful as a rapid annealing method in semiconductor device fabrication.

4. Conclusions

We investigated the activation of silicon implanted with phosphorus and boron atoms by microwave annealing using a commercial 2.45 GHz microwave oven. We carried out implantations of 1.0×10^{15} cm⁻² phosphorus atoms at 75 keV for p-type silicon substrates and 1.0×10^{15} cm⁻² boron atoms at 25 keV for n-type silicon substrates. Microwave irradiations with a power of 1000 W and duration of 120 s were subsequently conducted on the samples to activate the impurity atoms. During annealing, the silicon substrates were completely covered with carbon powder for effective heating and placed on the glass substrate with low heat conductivity to keep the heated energy in the sample region. Carbon powder effectively absorbed microwaves and heated itself at about 1000 °C. Optical reflectivity spectra were

measured to investigate the crystalline state in the surface implanted region. The silicon surface region was amorphized by both phosphorus and boron implantations. Microwave annealing caused recrystallization in the implanted region, although a small amount of slightly amorphized region still remained under the present annealing conditions. A 9.35 GHz microwave transmittance measurement revealed that the sheet resistivities of the phosphorus- and boron-implanted samples decreased to 140 and 85 Ω/sq , respectively, because of the increase in carrier density in the implanted surface region. We also used a microwave transmittance measurement system to precisely measure the τ_{eff} in the cases of CW 635 and 980 nm LD light illuminations. Experimental τ_{eff} values with the two different wavelength light illuminations to the top and rear surfaces were analyzed by numerical calculation with a finite-element program including models of photo-induced carrier generation, and their diffusion and annihilation with τ_b , S_{top} , and S_{rear} . Small S_{top} and S_{rear} values of 7.0 and 3.0 cm/s were obtained for the initial p- and n-type silicon samples, respectively, because both the silicon surfaces were well passivated by the thermally grown SiO_2 layers. On the other hand, S_{top} markedly increased to 5.0×10^4 and 5.0×10^3 cm/s for the phosphorus- and boron-as-implanted samples, respectively. This result shows that a substantial number of recombination defect states were generated in the silicon surface region by implantation. Microwave annealing at 1000 W for 120 s with carbon powder decreased S_{top} to 3.8×10^2 and 2.7×10^2 cm/s for the phosphorus- and boron-implanted samples, respectively. The density of recombination defect states caused by implantation was greatly decreased by microwave annealing. Typical diode rectified characteristics were observed for the sample activated by the present annealing method. Typical solar cell characteristics were also obtained by AM 1.5 light illumination at 100 mW/cm². I_{sc} , V_{oc} , FF, and conversion efficiency were 36 mA/cm², 0.52 V, 0.54, and 10.1%, respectively.

Acknowledgment

This work was partly supported by Grants-in-Aid for Scientific Research C (25420282 and 23560360) from the Ministry of Education, Culture, Sports, Science and Technology of Japan.

- 1) S. M. Sze, *Semiconductor Devices* (Wiley, New York, 1985) Chaps. 4–9.
- 2) M. Mehrotra, J. C. Hu, A. Jain, W. Shiau, V. Reddy, S. Aur, and M. Rodder, *IEDM Tech. Dig.*, 1999, p. 419.
- 3) T. Ito, K. Suguro, M. Tamura, T. Taniguchi, Y. Ushiku, T. Iinuma, T. Itani, M. Yoshioka, T. Owada, Y. Imaoka, H. Murayama, and T. Kusuda, *Ext. Abstr. 3rd Int. Workshop Junction Technology*, 2002, p. 23.
- 4) K. Ueda and M. Kasu, *Jpn. J. Appl. Phys.* **49**, 04DF16 (2010).
- 5) R. F. Wood and C. E. Giles, *Phys. Rev. B* **23**, 2923 (1981).
- 6) T. Sameshima, S. Usui, and M. Sekiya, *J. Appl. Phys.* **62**, 711 (1987).
- 7) A. Shima and A. Hiraiwa, *Jpn. J. Appl. Phys.* **45**, 5708 (2006).
- 8) T. Sameshima, M. Maki, M. Takiuchi, N. Andoh, N. Sano, Y. Matsuda, and Y. Andoh, *Jpn. J. Appl. Phys.* **46**, 6474 (2007).
- 9) K. Matsumoto, A. Ohta, S. Miyazaki, and S. Higashi, *Jpn. J. Appl. Phys.* **50**, 04DA07 (2011).
- 10) P. Kohli, S. Ganguly, T. Kirichenko, H. J. Li, S. Banerjee, E. Graetz, and M. Shevelev, *J. Electron. Mater.* **31**, 214 (2002).
- 11) K. Ukawa, Y. Kanda, T. Sameshima, N. Sano, and N. Hamamoto, *Jpn. J. Appl. Phys.* **49**, 076503 (2010).
- 12) T. Sameshima, K. Kogure, S. Yoshidomi, T. Haba, M. Hasumi, and N. Sano, *J. Laser Micro/Nanoeng.* **4**, 227 (2009).
- 13) T. Sameshima and N. Andoh, *MRS Proc.* **849**, KK9.5 (2004).
- 14) S. C. Fong, C. Y. Wang, T. H. Chang, and T. S. Chin, *Appl. Phys. Lett.* **94**, 102104 (2009).
- 15) P. Xu, C. Fu, C. Hu, D. W. Zhang, D. Wu, J. Luo, C. Zhao, Z. Zhang, and S. Zhang, *Appl. Phys. Lett.* **102**, 122114 (2013).
- 16) T. Sameshima, R. Ebina, K. Betsuin, Y. Takiguchi, and M. Hasumi, *Jpn. J. Appl. Phys.* **52**, 011801 (2013).
- 17) M. Hasumi, J. Takenezawa, T. Nagao, and T. Sameshima, *Jpn. J. Appl. Phys.* **50**, 03CA03 (2011).
- 18) A. Goldsmith, T. E. Waterman, and H. J. Hirschorn, *Handbook of Thermophysical Properties of Solid Materials* (Pergamon, New York, 1961) Vols. 1 and 3.
- 19) T. Sameshima, Y. Matsuda, Y. Andoh, and N. Sano, *Jpn. J. Appl. Phys.* **47**, 1871 (2008).
- 20) M. Born and E. Wolf, *Principles of Optics* (Pergamon, New York, 1974) Chaps. 1 and 13.
- 21) T. Sameshima, H. Hayasaka, and T. Haba, *Jpn. J. Appl. Phys.* **48**, 021204 (2009).
- 22) T. Sameshima, T. Nagao, S. Yoshidomi, K. Kogure, and M. Hasumi, *Jpn. J. Appl. Phys.* **50**, 03CA02 (2011).
- 23) T. Sameshima, Y. Takiguchi, T. Nagao, and M. Hasumi, *Proc. Workshop Active Matrix Flat Panel Displays*, 2012, p. 43.
- 24) A. S. Groove, *Physics and Technology of Semiconductor Devices* (Wiley, New York, 1961) Chap. 5.
- 25) T. Sameshima, K. Betsuin, T. Mizuno, and N. Sano, *Jpn. J. Appl. Phys.* **51**, 03CA04 (2012).
- 26) T. Sameshima, T. Nagao, M. Hasumi, A. Shuku, E. Takahashi, and Y. Andoh, *Jpn. J. Appl. Phys.* **51**, 03CA06 (2012).
- 27) H. H. Andersen and J. F. Ziegler, *Stopping and Ranges of Ions in Matter* (Pergamon, New York, 1977) Vol. 3.
- 28) Y. Taur and T. Ning, *Fundamental of Modern VLSI Physics* (Cambridge University Press, Cambridge, U.K., 1998) Chap. 2.
- 29) E. D. Palk, *Handbook of Optical Constants of Solids* (Academic Press, London, 1985) p. 547.
- 30) K. Winer, *Phys. Rev. B* **41**, 12150 (1990).